RSC Advances

ROYAL SOCIETY OF CHEMISTRY

www.rsc.org/advances

Graphic Abstract

Luminescent porous polymers based on octavinylsilsequioxane and triphenylamine units show tunable porosity and luminescence, a moderate uptake of CO_2 and high sensitivity for TNT.

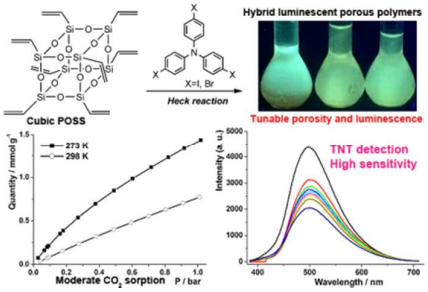

Cite this: DOI: 10.1039/c0xx00000x

www.rsc.org/xxxxxx

ARTICLE TYPE

POSS-Based Luminescent Porous Polymers for Carbon Dioxide Sorption and Nitroaromatic Explosives Detection†

Dengxu Wang,[a,b] Liguo Li,[b] Wenyan Yang,[b] Yujing Zuo,[b] Shengyu Feng,*[a,b] and Hongzhi Liu*[b]

Received (in XXX, XXX) Xth XXXXXXXXX 20XX, Accepted Xth XXXXXXXXX 20XX

DOI: 10.1039/b000000x

Luminescent hybrid porous polymers (LHPPs) have been synthesized by the Heck coupling reactions of cubic octavinylsilsequioxane (OVS) and halogenated triphenylamine (TPA). The resulting materials show high thermal stability and their porous and luminescent properties could be tuned by altering TPA species and reaction condition. The optimized polymer LHPP-3 exhibits high porosity with Brunauer–Emmer–Teller surface area of 680 m^2 g^{-1} and total pore volume of 0.41 cm^3 g^{-1}, and emits high yellow luminescence. LHPP-3 possesses a moderate CO_2 uptake of 1.44 mmol g^{-1} at 273 K and 0.77 mmol g^{-1} at 298 K at 1.01 bar, suggesting these polymers could be utilized as adsorbents for CO_2 storage and capture. Significantly, the luminescence of LHPP-3 could be quenched efficiently by nitroaromatic explosives such as 4-nitrotoluene, 2,4-dinitrotoluene and 2,4,6-trinitrotoluene, thereby indicating that the polymers could be utilized as chemical sensors for explosives detection.

Introduction

Covalently-linked luminescent porous polymers (LPPs) are an emerging class of functional materials with inherent porosity, luminescence and three-dimensional (3D) network structures.[1] Such materials have shown great potential applications in the fields of light emitting, light harvesting, optoelectronics and chemosensor, in addition to typical usage in gas storage, gas separation and heterogeneous catalysis.[1-3] LPPs materials are generally constructed from aromatic compounds because of their two characteristics, i.e., the rigid and contorted structures and π-electronic components.[1,2] The former one prevents the networks from collapsing and the space is filled in an efficient manner, thus resulting in porosity. The latter one ensures to form an extended π-conjugated network, which contributes to luminescence. For instance, Weber and Thomas reported the first example of blue light-emitting microporous polymers based on a spirobifluorene monomer.[4] Subsequently, several color-tunable conjugated microporous polymers (CMPs) were synthesized derived from phenyl,[5] pyrene,[6] carbazole,[7] and tetraphenylethene[8,9] units. An intriguing finding of these materials is that they exhibit an improved luminescence because the highly porous network can suppress chain aggregation.[1,8] This feature can efficiently conquer the disadvantage of conventional conjugated polymers, which have a tendency to aggregate in solutions and the solid state, possibly leading to emission quenching and limiting their utility as optical materials.[10] However, pure organic porous materials have their intrinsic limitations lacking both mechanical strength and thermal stability, which are disadvantageous for practical use.

The introduction of polyhedral oligomeric silsesquioxanes (POSS, typically $R_8Si_8O_{12}$) moieties into the organic networks could remarkably enhance the mechanical and thermal properties because of their inorganic-organic hybrid structures.[11] POSS have also been proved as ideal building blocks for the construction of porous polymers because they are rigid, high functional and exceptionally robust with respect to heat and water.[12] The cubic $R_8Si_8O_{12}$ unit can be regarded as structurally equivalent to the 4,4' (double four-ring) unit in the LTA and ACO topologies of zeolites, which provides the opportunities to prepare porous polymers with predictable structures.[13] Several POSS-based porous materials have been synthesized by diversified polymerizations including hydrosilation reaction,[14] Sonagashira reaction,[13] Yamamoto reaction,[15] Friedel-Crafts reaction,[16] Heck reaction,[17-19] and others.[20]

Moreover, the rigid and bulky POSS moieties have been incorporated into luminescent molecules and polymers to improve solubility and tune the photophysical properties.[21-23] One intriguing feature is that the introduction of POSS units can enhance their quantum yields due to suppression of self-quenching in the solid state. For example, dumbbell-shaped POSS derivatives linked by luminescent π-conjugated units gave transparent films and improved emission efficiency in the solid state compared with the model compounds.[22] Laine *et al.* found that POSS cores extended 3-D conjugation in the excited state for a set of stilbene-substitued POSS derivatives.[23] However, up to date, there is no report on the exploitation of POSS-incorporated LPPs materials except one preliminary research reported by us.[18]

Recently, we introduced Heck reaction to construct POSS-based porous polymers and found that their porous properties could be effectively tuned by altering monomer species, monomer structure and reaction condition.[17-19] The introduction of tetrahedral silicon-centered precursors into the networks resulted in POSS-based LPPs materials exhibiting blue luminescence.[18] However, tuning the optical properties of these

materials and their potential applications in chemosensor and related fields have not been investigated. Therefore, in the present study, we synthesized novel luminescent hybrid porous polymers, LHPP-1 to LHPP-3, using OVS and halogenated triphenylamine (TPA) as monomers via the Heck reaction (see Scheme 1). The selection of TPA as the luminescent unit is driven by the low-cost of TPA sources and excellent properties of TPA-containing functional materials including good hole-transport capabilities, efficient light emission, high photorefractivities and photoconductivities, *etc*.[24] Then porous and luminescent properties of the resulting polymers were investigated. The results showed that these two properties could be tuned by altering TPA species and reaction condition. Moreover, their applications in explosive detection and carbon dioxide sorption of LHPP-3 by the utilization of porosity and luminescence were investigated.

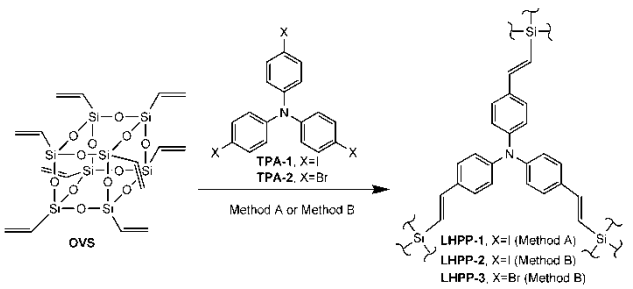

Scheme 1 Synthetic routes of luminescent hybrid porous polymers (LHPPs). Method A: $Pd(OAc)_2/PPh_3$, THF/Et_3N, 80ºC, 48h; Method B: $Pd(OAc)_2/P(o\text{-}CH_3Ph)_3$, DMF/$Et_3N$, 100ºC, 48h.

Results and Discussion

Synthesis and characterization

Luminescent hybrid porous polymers, LHPP-1 to LHPP-3, were synthesized by the Heck reaction of OVS and halogenated TPA (Scheme 1). Similar to our recent report,[19] the polymers derived from OVS and iodinated TPA (TPA-1) were prepared under two sets of conditions: One was at 80ºC in THF using $Pd(OAc)_2/PPh_3$ as the catalyst for 48 h (method A); Another was at 100°C in DMF using $Pd(OAc)_2/P(o\text{-}CH_3Ph)_3$ as the catalyst for 48 h (method B). Thus two polymers, i.e., LHPP-1 and LHPP-2, were afforded from method A and method B, respectively. The polymer LHPP-3 derived from OVS and brominated TPA (TPA-2) was prepared under method B. After the reactions, the crude products were recovered by filtration, washed and extracted with several solvents, and dried under vacuum at 70 ºC for 48 h to yield the materials. The coupling degrees for LHPP-1 to LHPP-3 were 96.9%, 98.1%, and 98.5%, respectively, as calculated by elemental analysis of the C, O, Si, X (X = Br or I) contents based on energy dispersive X-ray spectrometry (EDS) results (Fig. S1).

In order to confirm their structures, the polymers were characterized by FTIR, solid-state ^{13}C CP/MAS NMR and ^{29}Si MAS NMR spectroscopy. As the polymers had similar chemical structures, LHPP-1 was selected as a representative example. Fig. 1a and Fig. S2 show the FTIR spectra of OVS and LHPP-1. The C=C stretching vibration peaks from vinyl and phenyl groups for LHPP-1 were observed at 1411, 1505 and 1598 cm^{-1}. The characteristic Si-O-Si stretching vibration peak for LHPP-1 appeared at ca. 1110 cm^{-1}, which was broader than that of OVS, indicating the presence of cross-linking networks.[13-20]

Fig. 1b and Fig. 1c show the solid-state ^{13}C CP/MAS NMR and ^{29}Si MAS NMR spectroscopy of LHPP-1. The assignments of resonance signals for the polymer were straightforward based on our recent reports.[17-19] The ethenylene units confirming the formation of internal double bonds between vinyl and halogenated phenyl units in the structure showed peaks at ca. 119 ppm and 148 ppm. The signals from phenylene carbon atoms were observed 128 ppm, 136 ppm and 148 ppm. The peaks from phenylene and ethenylene units at 148 ppm were overlapped. The solid-state ^{29}Si NMR spectrum showed two signals at -68.2 ppm and -77.7 ppm, which were attributed to T_2 and T_3 units (T_n: $CSi(OSi)_n(OH)_{3-n}$) in the framework. This finding confirms the presence of POSS moieties and indicates that partial POSS cages collapsed during synthesis, consistent with other POSS-based porous polymers.[13,15,17-19] In addition, Q_n ($Si(OSi)_n(OH)_{4-n}$) species in the range of 90~120 ppm were observed, suggesting that partial Si-C bonds have been also cleaved. Such destructions were caused by the employment of the basic environment, i.e., triethylamine, and the distortion of cubic POSS cages linked by rigid connections to form cross-linking networks.[17-19] However, most of the cages remained intact in the networks.

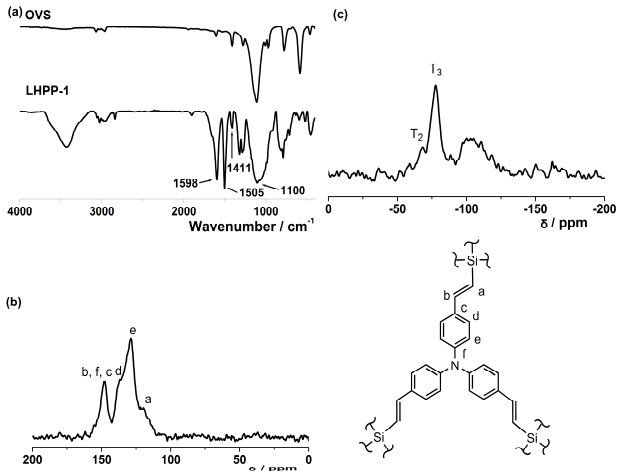

Fig. 1 (a) FTIR spectra of OVS and LHPP-1; (b) Solid-state ^{13}C CP/MAS NMR spectrum of LHPP-1; (c) solid-state ^{29}Si MAS NMR spectrum of LHPP-1.

Porosity

The porous properties of the polymers were investigated by nitrogen adsorption and desorption measurements at 77 K. The nitrogen isotherms of the polymers are shown in Fig. 2a and Table 1 summarizes the porosity data of each polymer. LHPP-1 showed a combination of type I and II nitrogen isotherms, while LHPP-2 and LHPP-3 gave rise to type I nitrogen isotherms according to the IUPAC classification.[25] All the isotherms displayed a sharp uptake at low relative pressures and then a gradually increasing uptake at higher pressures with hysteresis, thereby indicating the presence of micropores and mesopores within the structures. The slight increase in the nitrogen isotherm of LHPP-1 at a high pressure above 0.9 could be explained by condensation of nitrogen in the meso- and macrostructures of the samples and interparticular voids.[9,26]

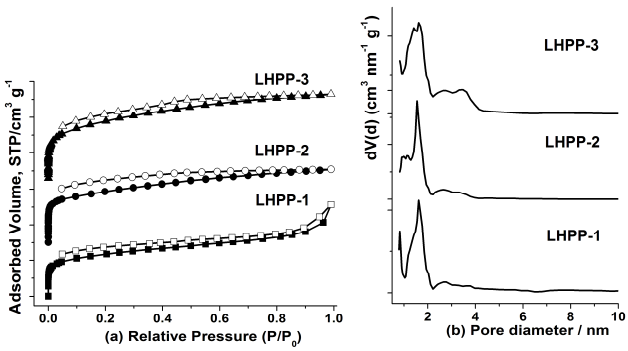

Fig. 2 (a) Nitrogen adsorption (closed symbols) and desorption (open symbols) isotherms for LHPP-1 to LHPP-3. For clarify, LHPP-2 and LHPP-3 are shifted vertically by 150 $cm^3\ g^{-1}$ and 300 $cm^3\ g^{-1}$; (b) pore size distribution curves of LHPP-1 to LHPP-3.

Although these polymers had similar chemical structures, their porosities were dramatically different by selecting the monomer species and reaction condition. The BET surface area (S_{BET}) and the total pore volume (V_{total}) are 422 $m^2\ g^{-1}$ and 0.40 $cm^3\ g^{-1}$ for LHPP-1 derived from OVS and TPA-1 using method A. When method A was replaced by method B, a higher S_{BET} of 512 $m^2\ g^{-1}$ was found in the resulting polymer LHPP-2, which could be explained by the higher coupling efficiencies and the choice of solvent. It has been demonstrated that high level of coupling degree and the choice of DMF are beneficial to enhance the surface area and pore volume.[19,27] Herein, the coupling degree of LHPP-2 (98.1%) was higher than that of LHPP-1 (96.9%). DMF was selected in the synthesis of LHPP-2 while THF was used for LHPP-1. However, LHPP-2 showed slightly lower V_{total} of 0.31 $cm^3\ g^{-1}$ than LHPP-1. When TPA-1 was replaced by TPA-2 in method B, LHPP-3 presented a much higher surface area and pore volume with a S_{BET} of 680 $m^2\ g^{-1}$ and a V_{total} of 0.41 $cm^3\ g^{-1}$, although iodinated monomer shows higher reactivity than brominated monomer. We speculated this result may be due to the relatively smoother formation rate of porous network LHPP-3 by using brominated monomer (TPA-2), than LHPP-2 by using iodinated monomer (TPA-1). This speculation can be proved by the initial formation time of the cross-linking products, which was observed at ca. 0.5 h and 2 h for LHPP-2 and LHPP-3.

The micropore analysis is calculated by the *t*-plot method. The micropore surface areas (S_{micro}) are 250, 317 and 424 $m^2\ g^{-1}$ for LHPP-1, LHPP-2 and LHPP-3. The micropore volumes (V_{micro}) are 0.13, 0.14 and 0.19 $cm^3\ g^{-1}$ for LHPP-1, LHPP-2 and LHPP-3. The ratios of V_{micro}/V_{total} are 0.32, 0.45 and 0.47 for LHPP-1, LHPP-2 and LHPP-3. The higher microporosity of LHPP-2, LHPP-3 than LHPP-1 further proved that DMF was a positive factor to increase the level of microporosity.[19,27] The pore size distributions (PSDs) were evaluated by nonlocal density functional theory (NL-DFT). As shown in Fig. 2b, LHPP-1 possessed uniform micropore with an average diamerer centered at ca. 1.61 nm and 0.90 nm. LHPP-2 showed more uniform micropore distribution with a diameter of 1.54 nm and two shoulders at 0.98 nm and 1.12 nm. Compared with LHPP-1 and LHPP-2, LHPP-3 exhibited broader micropore distribution with diameters of 1.41 nm and 1.61 nm. In addition, all of the polymers showed weak peaks in the range of 2~5 nm. These results agreed with the shape of the nitrogen isotherms, suggesting that micropore and mesopore coexisted in the networks.

Table 1 Porosity data of LHPP-1, LHPP-2 and LHPP-3

LHPPs	S_{BET}[a]/ $m^2\ g^{-1}$	S_{micro}[b]/ $m^2\ g^{-1}$	V_{total}[c]/ $cm^3\ g^{-1}$	V_{micro}[d]/ $cm^3\ g^{-1}$	V_{micro}/V_{total}
LHPP-1	422	250	0.40	0.13	0.32
LHPP-2	512	317	0.31	0.14	0.45
LHPP-3	680	424	0.41	0.19	0.47

[a] Surface area calculated from N_2 adsorption isotherm using the BET method; [b] Microporous surface area calculated from N_2 adsorption isotherm using *t*-plot method; [c] Total pore volume calculated at P/P_0 = 0.99; [d] Micropore volume derived using the *t*-plot method based on the Halsey thickness equation.

Thermal analysis

The thermal stabilities of OVS and the polymers were evaluated by thermogravimetric analysis (TGA) under N_2 at 10 °C min^{-1} (Fig. 3). The sharp mass loss of OVS over 200 °C is attributed to volatilization, which is the evaporation or sublimation in nitrogen atmosphere.[16,28] The hybrid polymers showed high thermal decomposition temperatures with 5% mass temperatures (T_d) of 310 °C, 350 °C and 460 °C, respectively, for LHPP-1, LHPP-2 and LHPP-3. The different thermal stabilities among these polymers may be due to the different coupling degrees and condensation rates. Initial decomposition can be attributed to the destruction of organic moieties including ethenylene groups and TPA units. After that, the siloxane spacers started to decompose. These materials were more thermally stable than other TPA-based porous polymers.[29,30] For example, a luminescent porous polymer, COP-2 showed much lower decomposition with T_d of 150 °C; COP-2 was synthesized through self-condensation of TPA-2 by the Yamamoto reaction.[29] This result indicated that the introduction of POSS moieties could enhance the thermal stability. Additionally, these materials were also comparable to or more stable than other POSS-based porous polymers.[13-20]

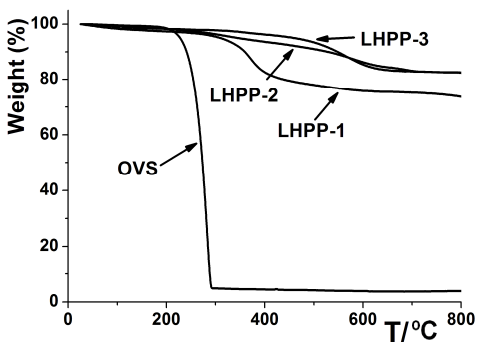

Fig. 3 TGA curves of OVS and LHPP-1 to LHPP-3 under N_2 at 10 °C min^{-1}

Morphology studies

As expected, power X-ray diffraction (PXRD) showed that the

LHPPs networks were amorphous and no evidence for characteristic reflections from long-range crystallographic order or layered sheets was observed (Fig. S4). The broad diffraction peaks centered at 2θ = 22° were undoubtedly associated with the Si-O-Si linkages.[13-20] To evaluate the particle size and morphology, field-emission scanning electron microscopy (FE-SEM) was performed. LHPP-1 consisted of relatively uniform solid submicrometer spheres (Fig. 4a). For LHPP-2 and LHPP-3, similar morphologies were observed (Fig. S5). The texture and ordering of the materials were performed by the high-resolution transmission electron microscopy (HR-TEM). The TEM image revealed that the polymer showed the characteristic of porous materials with a relatively uniform diameter, but no evidence of long-range ordering was observed (Fig. 4b, LHPP-1 as a representative example). The sample was stable under the electron beam.

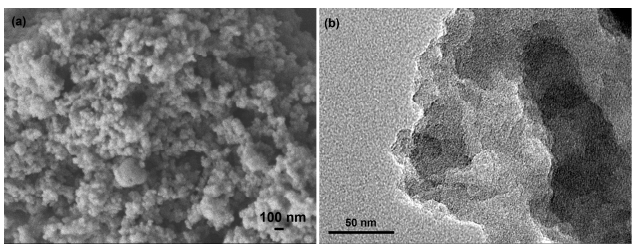

Fig. 4 (a) FE-SEM image of LHPP-1; (b) HR-TEM image of LHPP-1.

Photophysical properties

To investigate their potential applications in the optical area, UV-vis absorption and luminescent spectra of the polymers were measured. All the polymers showed a broad absorption across the wavelength range from 200 nm to 600 nm in the solid state (Fig. 5a). However, they showed different fluorescent emission in spite of having similar chemical structures. When excited at 365 nm in the solid state, LHPP-1 exhibited a broad emission band centered at 467 nm. The emissions for LHPP-2 and LHPP-3 were slightly red-shifted with respect to LHPP-1, with maximum emissions (λ_{max}) at 499 nm and 509 nm (Fig. 5b). Red-shifted emissions from LHPP-1 (λ_{max}: 479 nm) to LHPP-3 (λ_{max}: 499 nm) dispersed in THF were observed as well (Fig. 5c). Moreover, their luminescence could be visually observed under UV light and they all showed yellow luminescence (Fig. 5d-e). LHPP-3 gave the highest emission intensity, which is nearly threefold and ninefold compared with the intensities of LHPP-1 and LHPP-2 in the solid state and dispersed in THF, respectively (Fig. 5b-c). We speculated these results were attributed to the different coupling efficiencies and porosities of the materials. It has been demonstrated that the reaction efficiencies influenced the luminescent properties of the materials. For example, Jiang *et al.* have demonstrated that with reaction time increasing, the emission bands of the TPE-CMP samples were increasingly red-shifted from 538 nm (2 h) to 551 nm (72 h); TPE-CMP was synthesized using tetrakis(4-bromophenyl)ethene as a monomer by the Yamamoto reaction.[8] Herein, the coupling degrees for LHPP-2 and LHPP-3 were slightly higher than LHPP-1, thus resulting in a shortly red-shift of ca. 20~40 nm. Another important factor influencing the luminescence of the materials is the porosity, which can efficiently enhance the luminescent activity thanks to the interwoven porous network.[1,8] Therefore, LHPP-3 possessing the highest surface area and pore volume gave the best luminescent performance among these polymers.

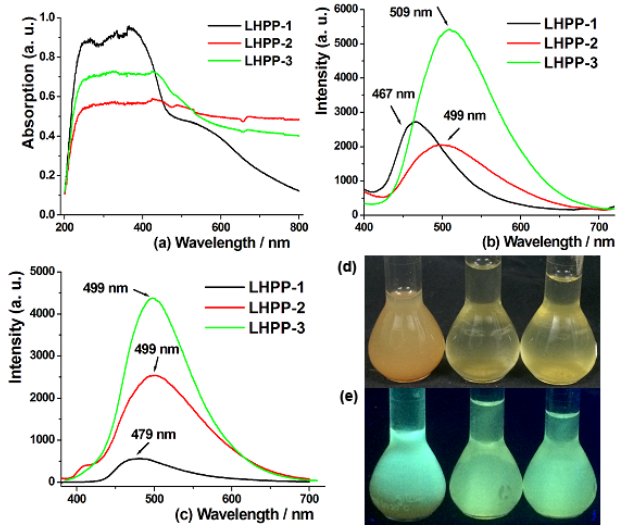

Fig. 5 UV-vis spectra (a) and Fluorescent spectra (b) of LHPP-1~LHPP-3 in the solid state; (c) Fluorescent spectra of LHPP-1~LHPP-3dispersed in THF (1 mg mL^{-1}, λ_{ex}=365 nm); Photographs of LHPP-1~LHPP-3 dispersed in THF without (d) and with (e) UV light irrdiation (365 nm).

These polymers showed red-shifted emissions compared to those of luminescent unit, i.e., TPA in the solid state (λ_{max}: 382 nm) and in THF solution (λ_{max}: 359 nm) (Fig. S6), which may be caused by two aspects: (i) the increased conjugated moieties; and (ii) structural defects that allowed some coupling between nearby phenyl rings since partial POSS cages were destructed in the network as proved by the solid-state ^{29}Si MAS NMR spectrum.[18] Compared with other TPA-based CMPs,[29,30] these polymers showed a slight blue-shift since the extended electronic conjugation was blocked by the inorganic POSS cages while the other CMPs network allowed for the extended electronic conjugation. To prove the blocking effect, molecular orbital calculation has been performed at the B3LYP/6-31G (d) level using Gaussian 03 suite of programs. Both of the highest occupied molecular orbital (HOMO) and lowest unoccupied molecular orbital (LUMO) were predominantly located on the TPA units and ethenylene units, thereby indicating POSS cages blocked the extended electric conjugation (Fig. S7).

Carbon dioxide sorption

In recent years, researchers have focused on the CO_2 adsorption because CO_2 is a key anthropogenic greenhouse gas and considered a threat to global warming.[31] Porous materials are a typical class of solid adsorbents.[32] In the present study, to evaluate the potential application of these polymers, CO_2 adsorption experiments at 273 K and 298 K were preformed and LHPP-3 was selected as an example. The uptakes of LHPP-3 were found to be 1.44 mmol g^{-1} (6.34 wt%) at 273 K and 0.77 mmol g^{-1} (3.39 wt%) at 298 K, which were measured up to 1.01 bar (Fig. 6a). This capacity is higher than that (1.38 mmol g^{-1} at 273 K and at 1 bar) of hybrid porous polymer (HPP-3) derived from OVS and 1,3,5-tribromobenzene although HPP-3 possessed higher surface area and pore volume (S_{BET}: 805 m^2 g^{-1}; V_{total}: 0.59 cm^3 g^{-1}).[19] This result may be due to the presence of triphenylamine units in the porous network. The chemical

functionality of the porous materials plays an important role in the CO_2 adsorption except the surface area and pore volume. It is known that the introduction of functional groups such as amine or carboxylic acid can improve CO_2 adsorption uptake.[33,34] For example, Cooper *et al.* have proved that the triazine networks absorbed more CO_2 than the corresponding benzene analogues despite having similar surface areas.[34] Therefore, herein the introduction of aromatic amine in LHPP-3 led to higher CO_2 adsorption than that for HPP-3. In addition, this uptake was also comparable to the corresponding values of some MOFs materials,[35] COFs materials[36] and porous polymers[37] with a level of surface areas. Compared with other porous organic polymers for CO_2 capture,[38] this uptake is relatively low, which is apparently due to the relatively low surface area. The coverage-dependent isosteric heat of CO_2 adsorption (Q_{st}) for LHPP-3 was calculated from the respective adsorption isotherms at 298 K and 273 K employing the Clausius-Clapeyron equation. As shown in Fig. 6b, the adsorption enthalpy was high (~29.6 kJ mol^{-1}) at low coverage, reflecting a strong CO_2-framework interaction, and gradually dropped at the increasing coverage. These results indicated that the materials could be potentially utilized as adsorbents for storing and capturing CO_2.

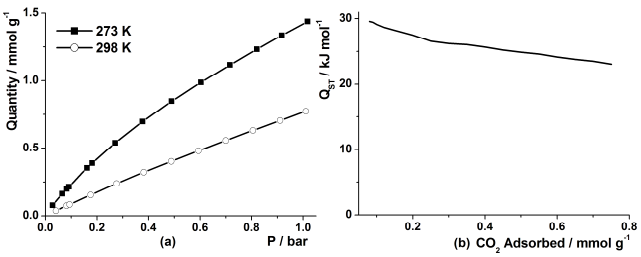

Fig. 6 (a) Carbon dioxide adsorption isotherms of LHPP-3 at 273 K and 298 K; (b) Isosteric heat of carbon dioxide adsorption of LHPP-3.

Explosive detection

Detecting nitroaromatic explosives has attracted much attention for military security and public safety. It is significant to detect explosives in a solution besides in vapour film because the residuals of explosives and their derivatives in the environment, such as from soil, groundwater and wastewater, are potentially harmful to humans, animals and plants. An efficient methodology is through fluorescence quenching based on luminescent materials.[39] Compared with the traditional organic luminescent molecules and polymers, an advantage of luminescent porous polymers is that they could be recycled because of the insolubility in common solvents.[30]

In the present study, the strong luminescence of LHPP-3 in the solid state and THF promoted us to explore its application for explosive detection, which was performed by adding successive concentrations of the analytes into LHPP-3 dispersed in THF. Fig. 7a-c show the quenching of luminescent spectra with three nitroaromatic compounds including NT, DNT and TNT. The fluorescence quenching could be easily discerned at low concentrations for all these analytes. The emission of LHHP-3 gradually became weak when the concentrations of analytes were increased. It was noted that LHPP-3 exhibited high sensitivity for TNT at low concentration (<1 ppm).

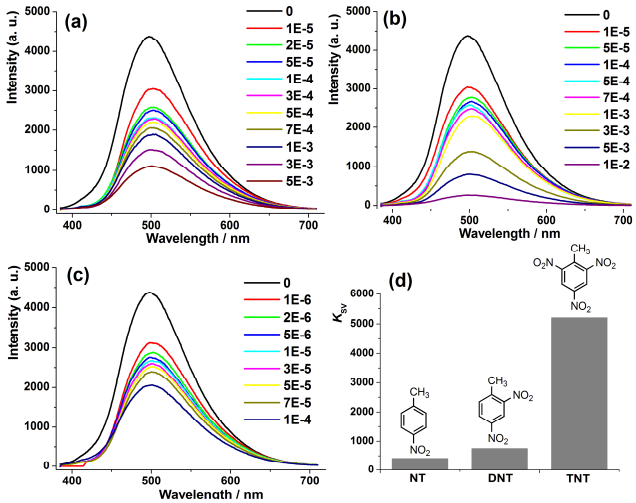

Fig. 7 (a-c) Quenching of luminescent spectra of LHPP-3 with various concentrations of NT (a), DNT (b) and TNT (c) in THF (1 mg mL^{-1}, λ_{ex}=365 nm). In each graph, the data for cutline refers to the concentrations of each analyte with M unit, and 0 refers to luminescent spectra without analyte. (d) The Stern-Volmer constants with NT, DNT and TNT analytes for LHPP-3.

The quenching efficiencies were calculated by the Stern-Volmer equation. As shown in Fig. S8, nearly linear Stern-Volmer plots were observed for all the analytes and the Stern-Volmer constants (K_{SV}) were 411 M^{-1}, 751 M^{-1} and 5208 M^{-1} for NT, DNT and TNT, respectively. The order of the quenching efficiencies is TNT>DNT>NT (Fig. 7d), which can be explained by the donor-acceptor electron-transfer mechanism.[29,40] Upon excitation, electrons are transferred from conduction band of LHPP-3 to the LUMOs of the analytes, leading to the quenching phenomenon. With the increase of electron withdrawing groups, i.e., -NO_2 in analytes, the quenching efficiencies are therefore enhanced. The order of LUMO levels of explosives is NT>DNT>TNT (Fig. S8 and Table S1), thus resulting in the transferred electron efficiency following the order of TNT> DNT>NT. In addition, the value of K_{SV} for TNT is also higher than or comparable to other luminescent porous polymers, some small molecules and conjugated polymers.[29,41] These results revealed that LHPP-3 could be potentially applied as a promising candidate to detect TNT explosives.

Conclusion

In summary, a series of POSS-based luminescent hybrid porous polymers, LHPP-1 to LHPP-3, have been prepared successfully using octavinylsilsequioxane (OVS) and halogenated triphenylamine (TPA) as monomers via the Heck reaction. Compared with other organic LPPs materials, the resulting hybrid materials showed high thermal stability and comparably high porosity with BET surface area up to 680 m^2 g^{-1}, indicating that incorporation of POSS moieties could enhance the thermal stability. Interestingly, both porosity and luminescence of the materials could be efficiently tuned by altering the TPA species and reaction condition. LHPP-3 with the highest porosity gave rise to the best luminescent performance, further proving that increasing porosity can enhance the luminescence due to the interwoven porous network. CO_2 adsorption and explosives

detection experiments of LHPP-3 revealed that these materials might be a kind of candidates for CO_2 storage and capture, as well as detecting nitroaromatic explosives.

Experimental Section

Materials

Unless otherwise noted, all reagents were obtained from commercial suppliers and used without further purification. OVS was synthesized by the previous report.[42] Tetrahydrofuran (THF) was dried by distillation over sodium metal prior to use. *N*,*N*-dimethylformamide (DMF) was first dried over CaH_2 at 80 ºC for 12 h, distilled under vacuum pressure and stored with 4 Å molecule sieves prior to use. Triethylamine (Et_3N) was dried over CaH_2 and used freshly.

Characterization

Fourier transform infrared (FTIR) spectra of the products were recorded on a Bruker Tensor27 spectrophotometer. Solid-state ^{13}C cross-polarization/magic-angle-spinning (CP/MAS) NMR and ^{29}Si MAS NMR spectra were performed on Bruker AVANCE-500 NMR Spectrometer operating at a magnetic field strength of 9.4 T. The resonance frequencies at this field strength were 125 and 99 MHz for ^{13}C NMR and ^{29}Si NMR, respectively. A chemagnetics 5 mm triple- resonance MAS probe was used to acquire ^{13}C and ^{29}Si NMR spectra. ^{29}Si MAS NMR spectra with high power proton decoupling were recorded using a $\pi/2$ pulse length of 5 μs, a recycle delay of 120 s and a spinning rate of 5 kHz. Elemental analyses were conducted using an Elementar vario EL III elemental analyzer. Elemental analyses were also performed using Oxford INCA X-sight energy dispersive X-ray spectrometry.

Field-emission scanning electron microscopy (FE-SEM) experiments were performed by using HITACHI S4800 Spectrometer. The high-resolution transmission electron microscopy (HR-TEM) experiments were performed by using a JEM 2100 electron microscope (JEOL, Japan) with an acceleration voltage of 200 kV.

Thermogravimetric analyses were performed with a MettlerToledo SDTA-854 TGA system in nitrogen at a heating rate of 10 ºC min^{-1} to 800 ºC. Powder X-ray diffraction (PXRD) were performed using a Riguku D/MAX 2550 diffractometer under Cu-Kα radiation, 40 kV, 200 mA with a scanning rate of 10 ° min^{-1} (2θ).

Nitrogen sorption isotherm measurements were performed on a Micro Meritics surface area and pore size analyzer. Before measurement, samples were degassed at 100 ºC for least 12 h. A sample of ca. 100 mg and a UHP-grade nitrogen (99.999%) gas source were used in the nitrogen sorption measurements at 77 K and collected on a Quantachrome Quadrasorb apparatus. BET surface areas were determined over a P/P_0 range from 0.01 to 0.20. Nonlocal density functional theory (NL-DFT) pore size distributions were determined using the carbon/slit-cylindrical pore mode of the Quadrawin software. Carbon dioxide (CO_2) adsorption isotherms at 298 K and 273 K were measured on a Micrometrics ASAP 2020. Prior to the measurements, the samples were degassed at 150 °C for at least 10 h.

The UV-vis spectra were determined with TU-1901 double beam UV-vis spectrophotometer. The fluorescence spectra were determined with HITACHI F-7000 spectrophotometer.

Synthesis of luminescent hybrid porous polymers (LHPPs)

LHPP-1. OVS (632 mg, 1 mmol), palladium acetate (90 mg, 0.4 mmol), and triphenylphosphine (210 mg, 0.8 mmol) were added under argon in THF/Et_3N (45 mL/15 mL). The mixture was stirred and bubbled by argon under stirring for 0.5 h at room temperature and then tris(4-iodophenyl)amine (TPA-1) (1.66 g, 2.67 mmol) was added. The reaction mixture was then heated at 80 ºC for 48 h. After cooling to room temperature, the mixture was filtered and the residue was washed with THF, chloroform, water, methanol and acetone to remove amine salts, unconsumed monomers and catalyst residues. Further purification of the sample was carried out by extraction with THF for 24 h and methanol for 24 h. The product was recovered by filtration, and dried under reduced pressure at 70 ºC for 48 h. LHPP-1 was afforded as a khaki solid (1.40 g). Yield: 110%. Elemental analysis calc. (wt.%) for $C_{64}H_{48}N_{2.67}Si_8O_{12}$: C 60.47, H 3.81, N 2.94; Found C 51.51, H 3.94, N 2.31. Coupling degree: 96.9%.

LHPP-2. OVS (632 mg, 1 mmol), palladium acetate (90 mg, 0.4 mmol) and tris(2-methylphenyl)phosphine (193 mg, 0.94 mmol) were dissolved in a DMF/Et_3N solution (45 mL/15 mL) under argon. The mixture was stirred and bubbled by argon under stirring for 0.5 h at room temperature and tris(4-iodophenyl)amine (TPA-1) (1.66 g, 2.67 mmol) was added. The resulting mixture was then heated at 100 °C for 48 h and cooled to room temperature. The purification of the crude product was similar to that of LHPP-1. LHPP-2 was afforded as a gray-green solid (1.33 g). Yield: 105%. Elemental analysis calc. (wt.%) for $C_{64}H_{48}N_{2.67}Si_8O_{12}$: C 60.47, H 3.81, N 2.94; Found C 56.67, H 4.50, N 2.77. Coupling degree: 98.1%.

LHPP-3. The synthesis procedure and post-treatment of LHPP-3 were similar to those of LHPP-2 except that tris(4-iodophenyl)amine (TPA-1) was replaced by tris(4-bromophenyl)amine (TPA-2) (1.28 g, 2.67 mmol). LHPP-3 was afforded as a gray-green solid (1.30 g). Yield: 102%. Elemental analysis calc. (wt.%) for for $C_{64}H_{48}N_{2.67}Si_8O_{12}$: C 60.47, H 3.81, N 2.94; Found C 57.64, H 4.63, N 2.76. Coupling degree: 98.5%.

Nitroaromatic explosives detections

Dried LHPP-3 (5 mg) was added into 5 mL THF and the resulting suspension was dispersed with ultrasonic oscillation. To explore the sensing properties for nitroaromatic explosives, the fluorescence spectra of suspension of LHPP-3 (1 mg mL^{-1}) were recorded by successive addition of aliquots of 4-nitrotoluene (NT), 2,4-dinitrotoluene (DNT) or 2,4,6-trinitrotoluene (TNT).

Acknowledgements

This research was supported by the National Natural Science Foundation of China (21274080 and 21274081), the Key Natural Science Foundation of Shandong Province (ZR2011BZ001) and the Fundamental Research Funds of Shandong University (2014GN009).

Notes and references

[a] *National Engineering Technology Research Center for Colloidal Materials, Shandong University, Jinan 250100, P. R. China. Fax: +86 531 88564464; Tel: +86 531 88364866; E-mail: fsy@sdu.edu.cn*

[b] *Key Laboratory of Special Functional Aggregated Materials & Key Laboratory of Colloid and Interface Chemistry (Shandong University), Ministry of Education, School of Chemistry and Chemical Engineering,*

Shandong University, Jinan 250100, P. R. China. E-mail: liuhongzhi@sdu.edu.cn

† Electronic Supplementary Information (ESI) available: Energy dispersive spectroscopy (EDS) results, BET plots, and XRD patterns of LHPP-1~3, FE-SEM images of LHPP-2 and LHPP-3, fluorescent spectra of triphenylamine, Stern-Volmer plots for NT, DNT and TNT of LHPP-3, HOMO and LUMO calculations and energies of LHPP-3, NT, DNT and TNT, HOMO and LUMO orbital diagrams of LHPP-3. See DOI: 10.1039/b000000x/

1 A. Patra, U. Scherf, *Chem. Eur. J.*, 2012, **18**, 10074; Y. Xu, S. Jin, H. Xu, A. Nagai, D. Jiang, *Chem. Soc. Rev.*, 2013, **42**, 8012.

2 K. Zhang, B. Tieke, F. Vilela, P. J. Skabara, *Macro. Rapid Commun.*, 2011, **32**, 825; J. Brandt, J. Schmidt, A. Thomas, J. D. Epping, J. Weber, *Polym. Chem.*, 2011, **2**, 1950; D. Xiao, Y. Li, L. Liu, B. Wen, Z. Gu, C. Zhang, Y. S. Zhao, *Chem. Commun.*, 2012, **48**, 9519; J. L. Novotney, W. R. Dichtel, *ACS Macro Lett.*, 2013, **2**, 423.

3 S. Wan, J. Guo, J. Kim, H. Ihee, D. Jiang, *Angew. Chem. Int. Ed.*, 2009, **48**, 5439; Y. Yuan, H. Ren, F. Sun, X. Jing, K. Cai, X. Zhao, Y. Wang, Y. Wei, G. Zhu, *J. Phys. Chem. C*, 2012, **116**, 26431.

4 J. Weber, A. Thomas, *J. Am. Chem. Soc.*, 2008, **130**, 6334.

5 L. Chen, Y. Honsho, S. Seki, D. L. Jiang, *J. Am. Chem. Soc.*, 2010, **132**, 6742.

6 J.-X. Jiang, A. Trewin, D. J. Adams, A. I. Cooper, *Chem. Sci.*, 2011, **2**, 1777.

7 X. M. Liu, Y. H. Xu, D. L. Jiang, *J. Am. Chem. Soc.*, 2012, **134**, 8738.

8 Y. H. Xu, L. Chen, Z. Q. Guo, A. Nagai, D. L. Jiang, *J. Am. Chem. Soc.*, 2011, **133**, 17622.

9 Q. Chen, J. Wang, F. Yang, D. Zhou, N. Bian, X. Zhang, C. Yan, B. Han, *J. Mater. Chem.*, 2011, **21**, 13554.

10 R. H. Friend, R. W. Gymer, A. B. Holmes, J. H. Burroughes, R. N. Marks, C. Taliani, D. D. C. Bradley, D. A. Dos Santos, J. L. Brédas, M. Lögdlund, W. R. Salaneck, *Nature*, 1999, **397**, 121.

11 Q. Chen, R. Xu, J. Zhang, D. Yu, *Macromol. Rapid Commun.*, 2005, **26**, 1878; J. Huang, Y. Xiao, K. Mya, X. Liu, C. He, J. Dai, Y. P. Siow, *J. Mater. Chem.*, 2004, **14**, 2858; D.-R. Yei, S.W. Kuo, Y.-C. Su, F.-C. Chang, *Polymer*, 2004, **45**, 2633; J. Choi, A. F. Yee, R. M. Laine, Macromolecules, 2003, **36**, 5666.

12 R. M. Laine, M. F. Roll, *Macromolecules*, 2011, *44*, 1073; D. B. Cordes, P. D. Lickiss, F. Rataboul, *Chem. Rev.*, 2010, **110**, 2081; K. Tanaka, Y. Chujo, *J. Mater. Chem.*, 2012, **22**, 1733.

13 W. Chaikittisilp, A. Sugawara, A. Shimojima, T. Okubo, *Chem. Eur. J.*, 2010, **16**, 6006.

14 C. Zhang, F. Babonneau, C. Bonhomme, R. M. Laine, C. L. Soles, H. A. Hristov, A. F. Yee, *J. Am. Chem. Soc.*, 1998, **120**, 8380.

15 W. Chaikittisilp, A. Sugawara, A. Shimojima, T. Okubo, *Chem. Mater.*, 2010, **22**, 4841.

16 Y. Wu, D. Wang, L. Li, W. Yang, S. Feng, H. Liu, *J. Mater. Chem. A*, 2014, **2**, 2160.

17 D. Wang, L. Xue, L. Li, B. Deng, S. Feng, H. Liu, X. Zhao, *Macro. Rapid Commun.*, 2013, **34**, 861.

18 D. Wang, W. Yang, L. Li, X. Zhao, S. Feng, H. Liu, *J. Mater. Chem. A*, 2013, **1**, 13549.

19 D. Wang, W. Yang, S. Feng, H. Liu, *Polym. Chem.*, 2014, **5**, 3634.

20 M. F. Roll, J. W. Kampf, Y. Kim, E. Yi, R. M. Laine, *J. Am. Chem. Soc.*, 2010, **132**, 10171; I. Nischang, O. Brüggemann, I. Teasdale, *Angew. Chem. Int. Ed.*, 2011, **50**, 4592.

21 S. Zheng, H. Phillips, E. Geva, B. D. Dunietz, *J. Am. Chem. Soc.*, 2012, **134**, 6944.

22 H. Araki, K. Naka, *J. Polym. Sci. Part A: Polym. Chem.*, 2012, **50**, 4170.

23 R. M. Laine, S. Sulaiman, C. Brick, M. Roll, R. Tamaki, M. Z. Asuncion, M. Neurock, J.-S. Filhol, C.-Y. Lee, J. Zhang, T. Goodson, III, M. Ronchi, M. Pizzotti, S. C. Rand, Y. Li, *J. Am. Chem. Soc.*, 2010, **132**, 3708.

24 P. J. Low, M. A. J. Paterson, D. S. Yufit, J. A. K. Howard, J. C. Cherryman, D. R. Tackley, R. Brookc, B. Brown, *J. Mater. Chem.*, 2005, **15**, 2304; Z. Ge, T. Hayakawa, S. Ando, M. Ueda, T. Akiike, H. Miyamoto, T. Kajita, M. Kakimoto, *Adv. Funct. Mater.*, 2008, **18**, 584; C. S. Karthikeyan, H. Wietasch, M. Thelakkat, *Adv. Mater.*, 2007, **19**, 1091; W. Z. Yuan, R. Hu, J. W. Y. Lam, N. Xie, C. K. W. Jim, B. Z. Tang, *Chem. Eur. J.*, 2012, **18**, 2847.

25 K. S. W. Sing, D. H. Everett, R. A. W. Haul, L. Moscou, R. A. Pierotti, J. Rouquèrol, T. Siemieniewska, *Pure Appl. Chem.*, 1985, **57**, 603.

26 M. Rose, N. Klein, W. Böhlmann, B. Böhringer, S. Fichtner, S. Kaskel, *Soft Matter*, 2010, **6**, 3918.

27 R. Dawson, A. Laybourn, Y. Z. Khimyak, D. J. Adams, A. I. Cooper, *Macromolecules*, 2010, **43**, 8524; J. R. Holst, E. Stöckel, D. J. Adams, A. I. Cooper, *Macromolecules*, 2010, **43**, 8531.

28 A. Fina, D. Tabuani, F. Carniato, A. Frache, E. Boccaleri and G. Camino, *Thermochim. Acta*, 2006, **440**, 36.

29 Z. Xiang, D. Cao, *Macromol. Rapid Commun.*, 2012, **33**, 1184.

30 L. Sun, Z. Liang, J. Yu, R. Xu, *Polym. Chem.*, 2013, **4**, 1932.

31 G. Férey, C. Serre, T. Devic, G. Maurin, H. Jobic, P. L. Llewellyn, G. D. Weireld, A. Vimont, M. Daturi, J.-S. Chang, *Chem. Soc. Rev.*, 2011, **40**, 550; S. Choi, J. H. Drese, C. W. Jones, *ChemSusChem*, 2009, **2**, 796.

32 R. Dawson, A. I. Cooper, D. J. Adams, *Prog. Polym. Sci.*, 2012, **37**, 530; D. Wu, F. Xu, B. Sun, R. Fu, H. He, K. Matyjaszewski, *Chem. Rev.*, 2012, **112**, 3959.

33 R. Dawson, E. Stöckel, J. R. Holst, D. J. Adams, A. I. Cooper, *Energy Environ. Sci.*, 2011, **4**, 4239; S. Ren, R. Dawson, A. Laybourn, J. Jiang, Khimyak, Y. D. J. Adams, A. I. Cooper, *Polym. Chem.*, 2012, **3**, 928.

34 J. Li, G. Yang, L. Hou, L. Cui, Y. Li, Y.-Y. Wang, Q.-Z. Shi, *Dalton Trans.*, 2013, **42**, 13590.

35 A. Mallick, S. Saha, P. Pachfule, S. Roy, R. Banerjee, *J. Mater. Chem.*, 2010, **20**, 9073.

36 T. Fröschl, U. Hörmann, P. Kubiak, G. Kučrová, M. Pfanzelt, C. K. Weiss, R. J. Behm, N. Hüsing, U. Kaiser, K. Landfester, M. Wohlfahrt-Mehrens, *Chem. Soc. Rev.*, 2012, **41**, 5313.

37 R. Dawson, D. J. Adams, A. I. Cooper, *Chem. Sci.*, 2011, **2**, 1173.

38 Q. Chen, M. Luo, P. Hammershøj, D. Zhou, Y. Han, B. Wegge Laursen, C.-G. Yan, B.-H. Han, *J. Am. Chem. Soc.*, 2012, **134**, 6084; Z. Xiang, X. Zhou, C. Zhou, S. Zhong, X. He, C. Qin, D. Cao, *J. Mater. Chem.*, 2012, **22**, 22663; Z. Xiang, D. Cao, *J. Mater. Chem. A*, 2013, **1**, 2691.

39 A. Rose, Z. Zhu, C. F. Madigan, T. M. Swager, V. Bulovic, *Nature*, 2005, **434**, 876; S. W. Thomas III., G. D. Joly, T. M. Swager, *Chem. Rev.*, 2007, **107**, 1339; Y. Salinas, R. Martínez-Máñez, M. D. Marcos, F. Sancenón, A. M. Costero, M. Parraad, S. Gil, *Chem. Soc. Rev.*, 2012, **41**, 1261.

40 S. Pramanik, C. Zheng, X. Zhang, T. J. Emge, J. Li, *J. Am. Chem. Soc.*, 2011, **133**, 4153; S. J. Toal, W. C. Trogler, *J. Mater. Chem.*, 2006, **16**, 2871.

41 W. Zhang, L.-G. Qiu, Y.-P. Yuan, A.-J. Xie, Y.-H. Shen, J.-F. Zhu, *J. Hazard. Mater.*, 2012, *221–222*, 147; H. Sohn, M. J. Sailor, D. Magde, W. C. Trogler, *J. Am. Chem. Soc.*, 2003, **125**, 3821.

42 R. H. Baney, M. Itoh, A. Sakakibara, T. Suzuki, *Chem. Rev.*, 1995, **95**, 1409.